coatings

MDPI

Article

Improving the Processability of a One-Step Hydrophobic Coating for Hot-Dipped Galvanised Steel for Industrial Applications

Jamie Williams [1,*], Christian Griffiths [2], Tom Dunlop [2] and Eifion Jewell [2]

[1] Materials Research Centre, College of Engineering, Swansea University, Bay Campus, Fabian Way, Crymlyn Burrow, Swansea SA1 8EN, UK
[2] SPECIFIC, College of Engineering, Swansea University, Bay Campus, Fabian Way, Crymlyn Burrow, Swansea SA1 8EN, UK; c.m.griffiths@swansea.ac.uk (C.G.); t.o.dunlop@swansea.ac.uk (T.D.); e.jewell@swansea.ac.uk (E.J.)
* Correspondence: 821838@swansea.ac.uk

Abstract: Hydrophobicity on steel-based metallic surfaces provides an advantage in limiting corrosion and debris buildup on the surface, thereby, improving the substrate performance. An experimental investigation was conducted on the development of zinc stearate and silicon dioxide coatings on the surface of hot-dipped galvanised zinc-coated steel substrates, which could be used to induce superhydrophobicity. Under optimal formulation and processing conditions, a contact angle of 146° could be produced within a 120-min processing window. This represents a reduction in processing time of 67% over previous literature using similar chemistry. In addition, we proved that costly nano silicon dioxide can be replaced by lower cost micro silicon dioxide without decreasing the performance of the coating contact angle. Under standard accelerated exposure tests, the coating was shown to reduce oxide build up by a factor of 3 compared to uncoated galvanized steel.

Keywords: hydrophobic coating; functional coating; zinc stearate; hot-dipped galvanised steel

Citation: Williams, J.; Griffiths, C.; Dunlop, T.; Jewell, E. Improving the Processability of a One-Step Hydrophobic Coating for Hot-Dipped Galvanised Steel for Industrial Applications. *Coatings* **2022**, *12*, 895. https://doi.org/10.3390/coatings12070895

Academic Editors: Jing Yu and Fabio Palumbo

Received: 13 May 2022
Accepted: 20 June 2022
Published: 24 June 2022

1. Introduction

Zinc (Zn)-based galvanised steel coatings provide anodic corrosion protection to underlying steel substrates and have been used extensively in the automotive and construction industries. The zinc coating is applied to the steel strip at speeds of up to 200 m/min with commonly applied zinc coating weights of 275 g/m^2. Conversion coatings are typically employed to improve the atmospheric corrosion resistance by the formation of a non-conducting precipitate on the zinc substrate surface. These coatings have previously contained hexavalent-chromate, which provides excellent corrosion resistance but due to their toxicity have been replaced with phosphate- or titanate-based solutions [1,2]. However, recent research has focused on more environmentally friendly processes [3].

There has been growing interest in the use of hydrophobic coatings (HCs) to improve corrosion resistance of metallic substrates and to provide functionality, such as self-cleaning [4–9]. These coatings are inspired by the natural surface of lotus leaves, which have nano-structured surfaces coated with low-surface-energy materials that provide an interface between the coating and liquid [10]. The interface is created by retaining air within the nano-scale topography of the surface, which reduces the contact area of water droplets, producing a highly non-wetting, low adherence surface [6,7,11]. A superhydrophobic surface (SHS) refers to a surface with a contact angle of more than 150° [8,12,13]. SHSs have been shown to provide effective corrosion protection on a range of metallic substrates, such as steel [14,15], copper [16], magnesium [17] and zinc [9,18–21].

The preparation of superhydrophobic coatings on metallic substrates can be achieved using a variety of methods, such as electrodeposition, chemical etching and hydrothermal growth [7,22–25]. However, many of these methodologies require complex two-step processes that would be difficult to implement in an industrial application. Due to these

issues, there has been recent advances to develop simple one-step methods to produce a superhydrophobic surface. Li et al. implemented a one-step immersion method to produce a superhydrophobic coating on zinc using a solution of stearic acid containing silver nitrate [26].

The coating was applied at room temperature within 1 min, and the reported results indicated excellent corrosion protection; however, the use of silver nitrate would be prohibitive for industrial applications due to cost. Chen et al. used a rapid one-step electrodeposition process to produce a superhydrophobic coating on copper using a nickel chloride-based electrolyte solution. The resulting surface was reported to achieve up to a 164° contact angle and less than 2° rolling angle; however, the corrosion resistance was not reported [27].

Liang et al. produced a superhydrophobic coating on a zinc surface implementing a simple one-step hydrothermal growth technique using stearic acid and silicon dioxide (SiO_2) particles [13]. The authors reported excellent corrosion performance when the coating was immersed in aqueous sodium chloride solution and contact angle measurements were recorded of up to 160°. The zinc layer on the surface of hot-dipped galvanized (HDG) steel reacted with stearic acid to form low surface energy zinc stearate. The chemical reaction for this is observed below [13]:

$$Zn - 2\,e^- = Zn^{2+} \quad (1)$$

$$Zn^{2+} + 2\,CH_3(CH_2)_{16}COOH = Zn[CH_3(CH_2)_{16}COO]_2 + 2\,H^+ \quad (2)$$

However, the coating required up to 6 h to form, which would be impractical for industrial applications. The work described here employs a simple one-step hydrothermal growth method using stearic acid and silicon dioxide particles to produce a highly hydrophobic coating on a hot-dipped galvanised (HDG) steel. The methodology described by Liang et al. provides a foundation for further improvements to reduce the time required to produce a suitable coating, thereby, making the coating more appropriate for industrial applications [13].

Furthermore, the nano-SiO_2 used in the method proposed by Liang et al. is compared with fumed-SiO_2, which is more readily available and commonly used in organic coatings [28]. Corrosion resistance has previously been studied by Liang et al. using EIS and potentio-dynamic polarisation, and in comparison, an industrially relevant accelerated corrosion test was used here to corroborate these previously published results. This work aims to produce a simple one-step hydrophobic coating on a HDG steel substrate, which may be scalable for industrial applications.

2. Materials and Methods

2.1. Materials

Sodium hydroxide, hydrogen peroxide (30%), stearic acid and silicon dioxide (9–20 nm) were purchased from Sigma Aldrich (St. Louis, MO, USA), and ethanol was purchased from Fisher Scientific (Hampton, VA, USA). Fumed silicon dioxide (Aerosil 300, Essen, Germany, 0.2–0.3 µm) was obtained from Evonik. All chemicals used were of reagent grade. Hot-dipped galvanized (HDG) steel was provided by Tata Steel (Port Talbot, Wales) and cut into 10 × 10 mm samples for the initial systematic study. Later, samples were cut into 80 × 80 mm coupons to scale up the coating formulation and for humidity testing.

2.2. Methods

2.2.1. Coating Production

A one-step immersion method was used to coat HDG steel samples. First, the HDG samples were prepared by degreasing using ethanol. They were then submerged in 1 M sodium hydroxide solution for 15 s at 50 °C, which replicates the industrial cleaning process [29]. The coating formulation used either ethanol or isopropyl alcohol (IPA) as the solvent, which is given in Table 1. The formulation was prepared by adding 0.05 M stearic acid to 100 mL of the relevant solvent.

Table 1. Formulations used to produce hydrophobic coatings.

Formulation	Solvent	Molarity of Stearic Acid (M)	SiO_2 Size (nm)	NaOH Addition
1	Ethanol	0.05	200–300	✗
2	IPA	0.05	200–300	✗
3	Ethanol	0.05	200–300	✓
4	Ethanol	0.1	200–300	✗
5	Ethanol	0.2	200–300	✗
6	IPA	0.05	200–300	✓
7	IPA	0.1	200–300	✓
8	IPA	0.2	200–300	✓
9	Ethanol	0.05	9–20	✓
10	Ethanol	0.1	9–20	✓
11	Ethanol	0.2	9–20	✓
12	IPA	0.05	9–20	✓
13	IPA	0.1	9–20	✓
14	IPA	0.2	9–20	✓

Hydrogen peroxide (2 mL) was added dropwise to the formulation whilst magnetically stirred for 1 min. Silicon dioxide (1% wt.) was added to the formulation and magnetically stirred for 30 min to ensure the stearic acid was fully dissolved and the silicon dioxide was evenly dispersed. The particle size of silicon dioxide was a variable investigated, which can be seen in Table 1. The formulation was heated and held at 70 °C using a hotplate before HDG samples were immersed for up to 360 min. The samples were then removed, rinsed with ethanol and blown dry.

2.2.2. Characterization Techniques

Surface morphology and analysis of the hydrophobic surface has visualised using scanning electron microscopy (SEM) (Hitachi TM3000) (Tokyo, Japan) equipped with electron dispersive spectroscopy (EDS). The wettability of the surface was determined by analysing the contact angle (CA) of de-ionised water in contact with the coating film. The CA measurement system comprised of a camera, and FTA32 software 2.0 (FTA1000 manual system, First Ten Angstroms) (Portsmouth, VA, USA) for analysis with an error measure of $\pm 1^{\circ}$ under optimized illumination and optical conditions.

Fourier-transform infrared spectroscopy (FTIR) (PerkinElmer spectrum-100) (Waltham, MA, USA) and x-ray diffraction (XRD) (Bruker D8 Discover with copper source 40 kV and 40 mA) (Billerica, MA, USA) were used to characterise the surface chemical constituents. XRD was conducted with a glancing angle setup consisting of a 2° incidence angle in true parallel beam configuration and increments of 0.02°. Atomic force microscopy (AFM) (JPK nanowizard 3) (Berlin, Germany) was used to measure the topography of the substrate surface. Lastly, the corrosion resistance was evaluated via subjecting the samples to 1000 h humidity testing.

2.2.3. Initial Studies

An initial study investigated the feasibility of reducing the time required to produce a hydrophobic coating using the experimental procedure published by Liang et al. [13]. Samples of HDG steel were immersed in formulation 1 and removed at regular intervals. The initial study revealed that the time required to achieve a suitably hydrophobic surface using the parameters published by Liang et al. [13] was after an immersion time of 120 min whereby a contact angle of $>100^{\circ}$ was measured. The contact angle versus immersion time is given in Figure 1a. The 120 min required to produce a suitably hydrophobic coating is used as a minimum time for the systematic study with a maximum time of 360 min as published by Liang et al.

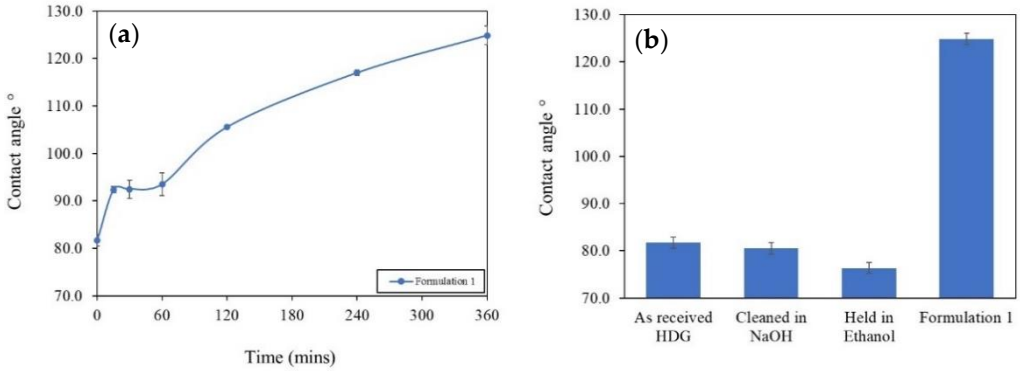

Figure 1. (**a**) CA vs. immersion time for formulation 1 over 360 min immersion, (**b**) recorded CA of HDG steel, which has been "as received", cleaned in NaOH, cleaned in NaOH and immersed in ethanol and cleaned and immersed in the coating formulation.

The contact angle of HDG steel samples with each surface treatment is shown in Figure 1b. There was very little change in CA for HDG samples that were cleaned or rinsed in ethanol compared to the as received HDG steel sample. However, there was a significant increase in CA (>120°) recorded for HDG steel immersed in formulation 1. This demonstrates that the surface cleaning conditions typically employed in industry do not contribute to increased CA.

The minimum time of 120 min was used in a systematic study to investigate variables including the solvent, the addition of NaOH, stearic acid molarity and SiO_2 particle size. Surface morphology and CA were assessed as a function of the formulation shown in Table 1. Throughout the systematic study, 14 formulations were investigated; however, the key findings and trends will be reported by examining a subset of these.

3. Results and Discussion

3.1. Surface Morphology and Wettability

The published methodology used by Liang et al. used ethanol to dissolve stearic acid. However, stearic acid has been shown to be more soluble in isopropyl alcohol (IPA) than in ethanol [30,31]. The increased solubility provided by using IPA would allow for higher concentrations of stearic acid to be used and may also have different morphology of the resultant hydrophobic coating when compared to that produced using ethanol.

Hydrophobic surfaces were produced through submerging HDG steel samples in formulations 1–3 given in Table 1 for up to 360 min. The surface morphology was observed using SEM imaging, which is shown in Figure 2a–d. Figure 2a shows a HDG steel surface that has been cleaned in 1 M sodium hydroxide solution for 15 s at 50 °C. Figure 2b–d shows that the surface morphology of the HDG steel dramatically alters after immersion in the experimental formulation compared to that of the cleaned HDG steel surface shown in Figure 2a. Figure 2b shows the surface morphology consists of lamellar structures when using ethanol as the solvent. Liang et al. reported similar structures in their work and suggested that the structures observed here are zinc stearate with silicon dioxide entrapped amongst the structure, shown by the lighter areas [13]. The surface morphology observed in Figure 2c is produced from formulation 2, whereby IPA is used as the solvent, replacing ethanol.

Here, the zinc stearate has formed in a dense needle-like precipitate compared to Figure 2b allowing larger floccules of silicon dioxide to be entrapped. Figure 2d shows the surface morphology produced from formulation 3, which is ethanolic-based containing an addition of 2% wt. 1 M NaOH (aq). The morphology shown here is similar to that shown in Figure 2b; however, the lamellar structures appear to be larger and less densely packed compared to that shown in the non-NaOH addition shown in Figure 2b.

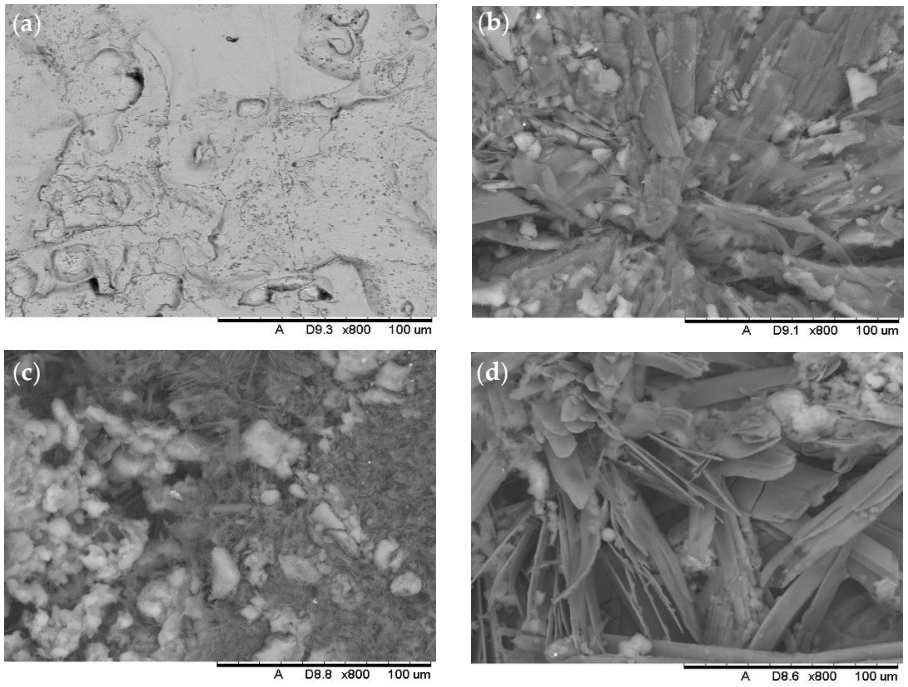

Figure 2. SEM images of fabricated coatings after immersion (**a**) uncoated, (**b**) formulation 1 (ethanol, 0.05 M stearic acid and micro-SiO_2) for 360 min, (**c**) formulation 2 (IPA, 0.05 M stearic acid and micro-SiO_2) for 360 min and (**d**) formulation 3 (ethanol, 2% wt. 1 M NaOH (aq), 0.05 M stearic acid and micro-SiO_2) for 360 min.

CA measurements for HDG steel samples immersed in formulations 1–3 for up to 360 min are shown in Figure 3. The maximum CA recorded for each sample generally occurred after 360 min of immersion with 125° for formulation 1, 135° for formulation 2 and 125° for formulation 3. The increase in CA recorded for formulation 2 can be attributed to the different surface morphology compared to that formed by samples immersed in formulation 1 or 3. Studying Figure 2b,c, the morphology is significantly altered when using IPA as a solvent compared to that of ethanol. The dense needle-like precipitate entraps more silicon dioxide and would provide a rougher surface, which could explain the increase in CA observed. Increased surface roughness can impart functionality to the surface via hydrophobicity. A higher density of surface features entraps air, which limits the liquid droplet's ability to rest on the surface and permeate through to the underlying substrate. This increase in surface roughness corresponds to an increase in CA [32,33].

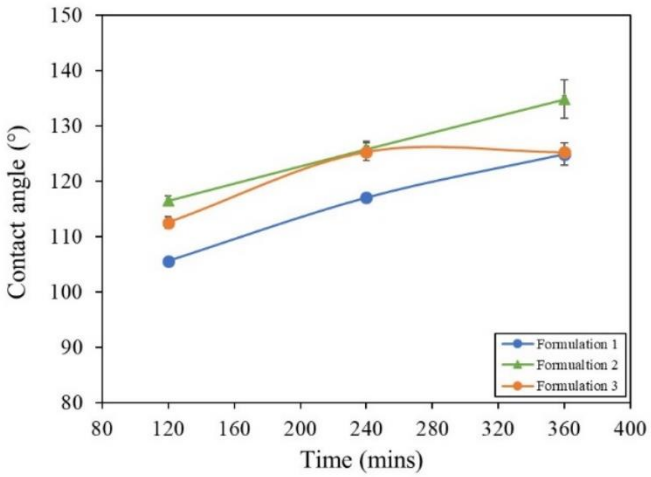

Figure 3. Relationship between CA against immersion time for formulations 1–3 from Table 1.

Formulation 3 has an addition of 2% wt. 1 M NaOH (aq) compared to that of formulation 1. Figure 3 showcases the difference in coating homogeneity when an addition of 2% wt. 1 M NaOH is present within the coating formulation. NaOH was introduced to increase the pH, which acts to activate the HDG steel surface and assist in increasing the homogeneity of the coating across the substrate surface. Zinc stearate structures form in similar lamellar plate shapes to those formed from formulation 1.

The maximum CA recorded is the same as that for formulation 1, which can be explained by the very similar surface morphology. However, the main advantage of the addition of NaOH was that of improved coating homogeneity. The improved coating homogeneity can be attributed to the increased activation of the HDG surface through the introduction of NaOH [34]. Due to the increased homogeneity of coating formation, it was decided to include 2% wt. 1 M NaOH within all subsequent formulations (Figure 4).

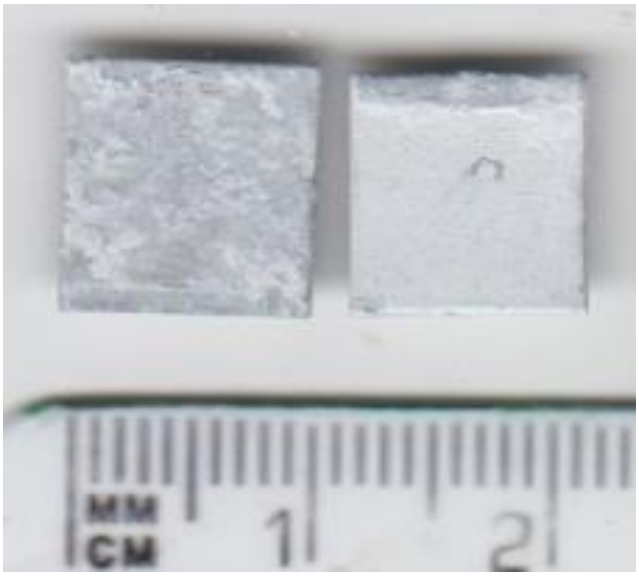

Figure 4. Image taken of hydrophobic samples coated with formulation 1 (**left**) and 3 (**right**) without and with 2% wt. 1 M NaOH addition, respectively.

Altering the molarity of stearic acid within the solution provided improved results by increasing surface CA whilst simultaneously decreasing immersion time. Additions of Stearic acid at concentrations of 0.05, 0.1 and 0.2 were evaluated within ethanol and IPA. Figure 5a–c shows the increase in molarity visibly affects the crystalline structure formed after a 360-min immersion period. Molarity increases over the three samples showed zinc stearate transition from needle-like structures to form lamellar structures. There is an increase in the population of zinc stearate and SiO_2 over the sample's surface, filling in open crevices left within the coating. CA measurements, shown in Figure 6, show that 0.2 M gave a negligibly higher CA in comparison to 0.1 and 0.05 M, recorded at 128°, 127° and 126°, respectively, when immersed for 360 min.

However, with increased molarity, higher CA was achieved in a shorter immersion time. This is demonstrated by formulations 7 and 8. Formulation 8 returned the greatest CA of 146°, in an immersion time of 120 min. Reducing the immersion time required to produce the coated surface is a crucial factor in improving the coating's industrial viability. Figure 6d shows the surface morphology of this sample, zinc stearate is formed in needle-like structures encapsulating floccules of SiO_2. The smaller needle structures are distributed more evenly across the surface, thereby, achieving better coating surface homogeneity. This enables air to be retained between zinc stearate and SiO_2 molecules. In turn, this contributes to a rougher surface that stops water droplets from permeating between pores, increasing the CA measured and surface hydrophobicity [13,35].

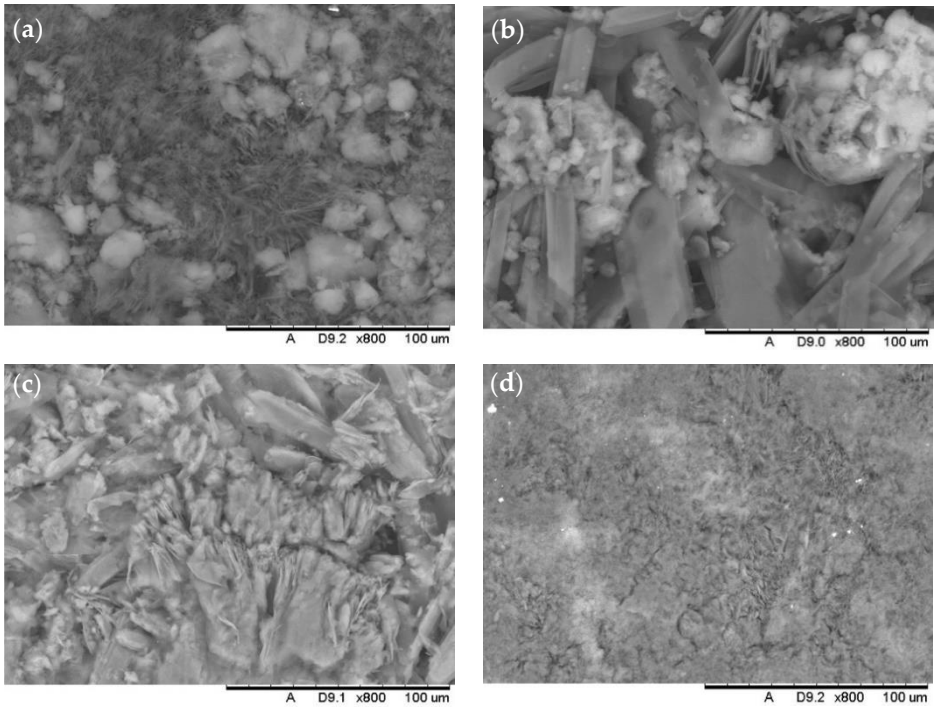

Figure 5. SEM images of fabricated coatings after immersion in (**a**) formulation 6 (IPA, 2% wt. 1 M NaOH (aq), 0.05 M stearic acid and micro-SiO_2), (**b**) formulation 7 (IPA, 2% wt. 1 M NaOH (aq), 0.1 M stearic acid and micro-SiO_2), (**c**) formulation 8 (IPA, 2% wt. 1 M NaOH (aq), 0.2 M stearic acid and micro-SiO_2) all for 360 min and (**d**) formulation 8 (IPA, 2% wt. 1 M NaOH (aq), 0.2 M stearic acid and micro-SiO_2) for 120 min.

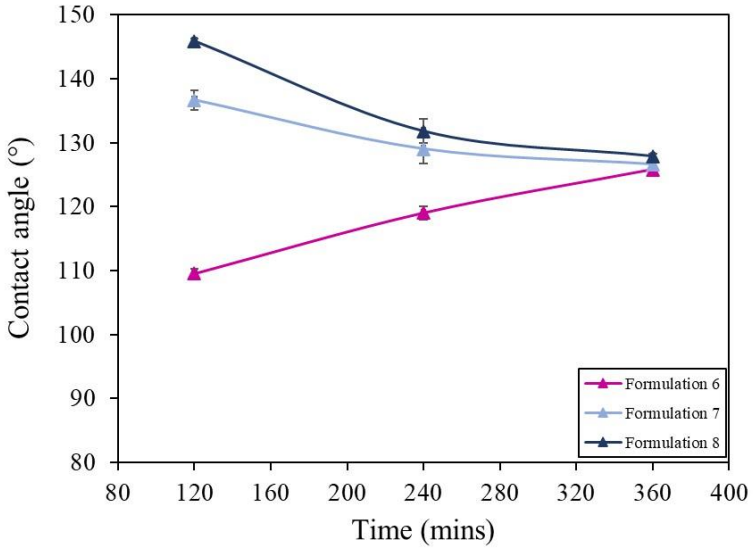

Figure 6. Relationship between CA against immersion time for formulations 6–8 from Table 1.

The particle size of additive SiO_2 was also assessed. Particle sizes of 9–20 nm were used, compared to the 0.2–0.3 µm that was used throughout the systematic study. Figure 7 demonstrates that a similar trend was found between CA and immersion time for the nanoparticles and microparticles of SiO_2. When the molarity is low, there is a positive relationship between immersion time and CA. As the molarity is increased, the initial CA is found to be higher but then decreases with increased immersion time. This is demonstrated by formulation 12, which has a CA of 118° and 129° at 120 and 360 min, respectively. In comparison, formulation 14 has a CA of 135° and 131° at 120 and 360 min, respectively.

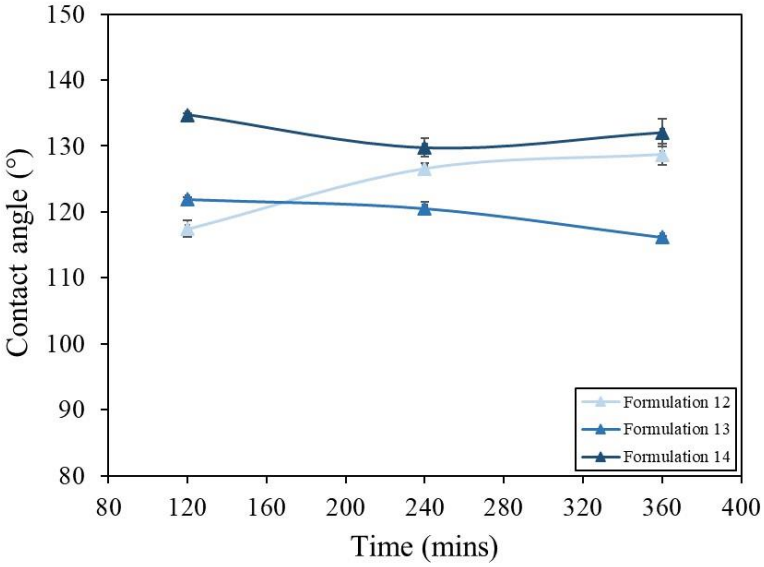

Figure 7. Relationship between CA against immersion time for formulations 12–14 from Table 1.

One theory for why CA decreases with increased immersion time is due to the SiO_2 formation blanketing the crystalline structure on the substrate surface. Increased SiO_2 deposition leads to decreased surface roughness and contributes to reducing the hydrophobicity of the substrate surface over time. The surface morphology is demonstrated in Figure 8a,b, and the change in structure with increased immersion time is attributed to the increased SiO_2 deposition. AFM was utilised to validate this theory by evaluating the surface roughness of the specimens from formulation 8 at 120 min and formulation 14 at 120 and 360 min. When analysing the data on formulation 14 from Table 2, we observe that the roughness values decreased between the two samples. This validates the previous assumption showing that hydrophobicity can be negatively impacted in comparison to when lower concentrations are used within solution. The AFM maps for the surface roughness are shown in Figure 9.

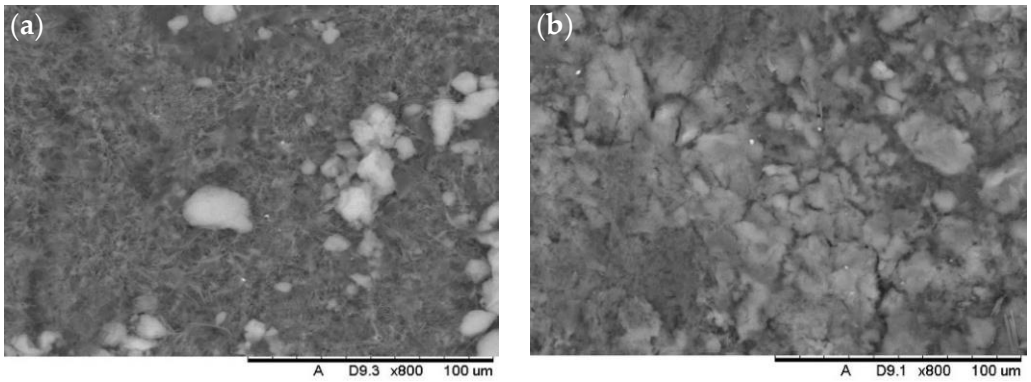

Figure 8. SEM images of fabricated coatings after immersion in formulation 14 (IPA, 2% wt. 1 M NaOH (aq), 0.2 M stearic acid and nano-SiO_2) for (**a**) 120 min and (**b**) 360 min.

Table 2. Surface roughness data via AFM from samples coated in formulation 8 and 14.

Surface Roughness	Formulation 8	Formulation 14	
	120 min	120 min	360 min
Average, S_a	194 nm	77 nm	47 nm
RMS, S_q	243 nm	101 nm	64 nm

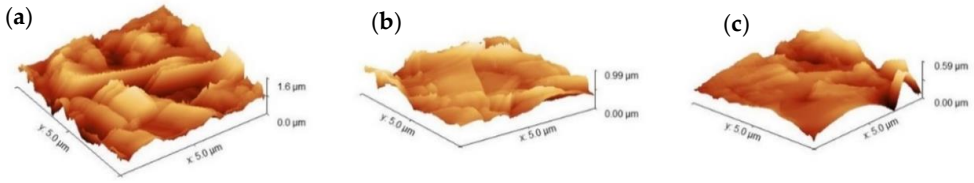

Figure 9. Topographical images produced by AFM of samples coated (**a**) in formulation 8 for 120 min, (**b**) formulation 14 for 120 min and (**c**) formulation 14 for 360 min.

3.2. FTIR Analysis

FTIR analysis was conducted to determine the changes in the different functional groups that form due to the reaction of stearic acid and zinc. Figure 10 shows FTIR spectra for SiO_2, the hydrophobic surface formed and stearic acid. Peaks at 1099 and 810 cm^{-1} in Figure 10a relate to the symmetric and asymmetric stretching vibration of Si-O-Si bonds, whilst 462 cm^{-1} relates to the Si–O bending vibration absorption [36,37]. The 2915 and 2850 cm^{-1} peaks in Figure 10b,c correspond to C–H bonds on the hydrophobic surface and in stearic acid, respectively.

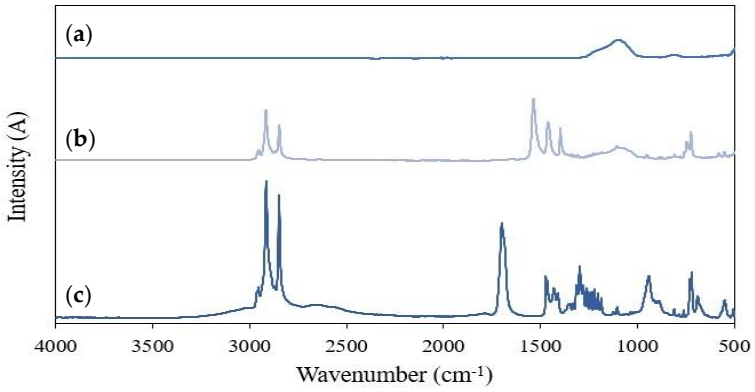

Figure 10. FTIR spectra of (**a**) SiO_2 (**b**) hydrophobic sample and (**c**) stearic acid.

Figure 10c shows peaks located at 1705 and 940 cm^{-1}, which represent C–O stretching vibration and the absorption peak of the hydroxyl group (–OH) in the carboxyl group (–COOH). These peaks are not present in Figure 10b and are instead replaced by peaks at 1540 and 1397 cm^{-1}. These changes demonstrate the –COOH present in stearic acid has changed, with H replaced by Zn [13,38]. This change demonstrates the preparation of the zinc stearate hydrophobic surface onto the HDG steel surface. The chemical reaction observed is stated in Equations (1) and (2).

3.3. Optimal Coating Parameters

We observed that the optimal coating system was shown to be formulation 8. This formulation consisted of 0.2 M stearic acid, 1% wt. SiO_2 (0.2–0.3 µm), 2% wt. 1 M NaOH and was immersed for 120 min achieving a mean contact angle of 146°. This system provided the most hydrophobic surface as well as demonstrating a more homogeneous coating throughout.

3.4. Humidity Testing

3.4.1. Method and Results

Potentiodynamic polarisation and EIS were previously used by Liang et al. to characterise similar coatings to those in the work described here. They reported that the hydrophobic coating increased the electrode potential and reduced the corrosion current density indicating an improvement in the corrosion resistance. Equivalent circuits also demonstrated that the coated samples produced larger charge transfer resistance compared to uncoated zinc, which represents the flower corrosion processes observed [13].

High humidity can cause failure of metal substrates, and thus high humidity environments are utilised to assess the corrosion performance of a substrate. Conditions can be mimicked closely within laboratory settings using a humidity cabinet. Samples were placed at 45° and held at 35 °C and 100% humidity as per Standard ASTM D2247-15. Formulation 8 was utilised to fabricate the hydrophobic surface on HDG steel coupons measuring 80 mm × 65 mm.

The investigation was conducted for up to 1000 h. At intervals of 0, 250, 500 and 1000 h a canon EOS 5D camera within a lightbox was used to photograph the samples, mass measurements were taken of each sample. Epoxy resin was used to seal the cut edges of the samples, and the water uptake of the resin was negated for and deducted from the final mass change values to achieve accurate and concurrent readings. Figures 11a–d and 12a–d show photographs taken of the uncoated and coated samples throughout humidity testing.

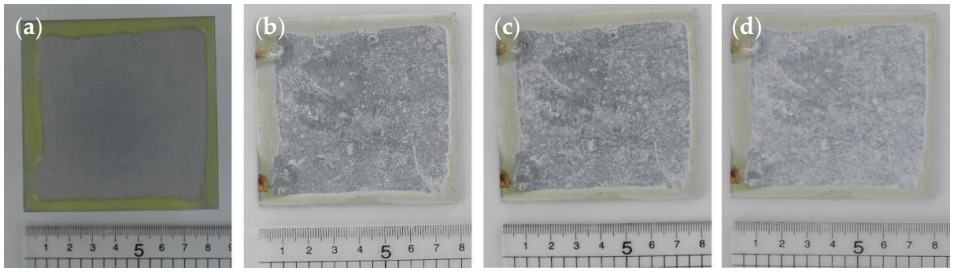

Figure 11. Humidity samples of uncoated HDG at (**a**) 0 h (**b**) 250 h (**c**) 500 h and (**d**) 1000 h.

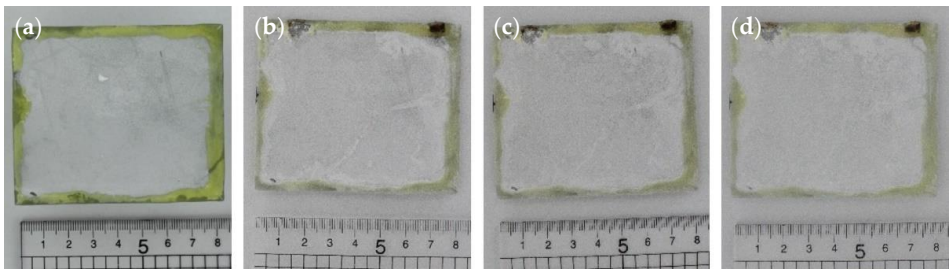

Figure 12. Humidity samples of coated HDG at (**a**) 0 h (**b**) 250 h (**c**) 500 h and (**d**) 1000 h.

Figure 13 demonstrates the increase in mass gained by both sample sets over this period. The uncoated sample visibly changes as a white precipitate is formed across the substrate surface. In contrast, the coating layer formed from zinc stearate and SiO_2 does not significantly change over the testing period. The mass change differences showcase the coated sample sees a significantly reduced mass increase and thus a higher corrosion resistance when compared with the uncoated sample.

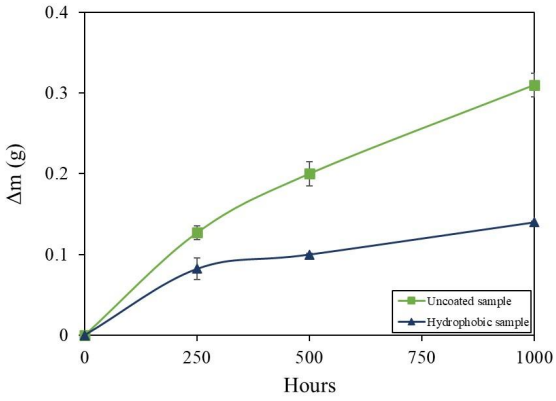

Figure 13. Mass gain of humidity samples over 1000 h displaying uncoated sample and hydrophobic sample.

3.4.2. XRD and FTIR Analysis of Humidity Results

Compositional analysis from XRD is given in Figure 14, which is used to determine the phase structure of the hydrophobic coating. A comparison is shown between the uncoated sample and the hydrophobic sample after 1000 h of humidity testing. By comparison, we observed that zinc stearate ($Zn(SA)_2$ where SA represents the stearate complex) is formed on the hydrophobic sample surface, and this signifies the reaction of zinc and stearic acid as shown in Equation (1). SiO_2 can also be seen in the XRD pattern, showcasing that SiO_2 has been encapsulated within the coating by physical action and not changing physical composition. The notable peak, which is observed in the uncoated sample and not the coated sample is that of zinc carbonate hydroxide and zinc hydroxide [6,13,39–41]. This is created via the mechanisms:

$$5\ ZnO + 2\ CO_2 + 3\ H_2O = Zn_5(CO_3)_2(OH)_6 \quad (3)$$

$$Zn + 2\ H_2O = Zn(OH)_2 + 2\ H_2 \quad (4)$$

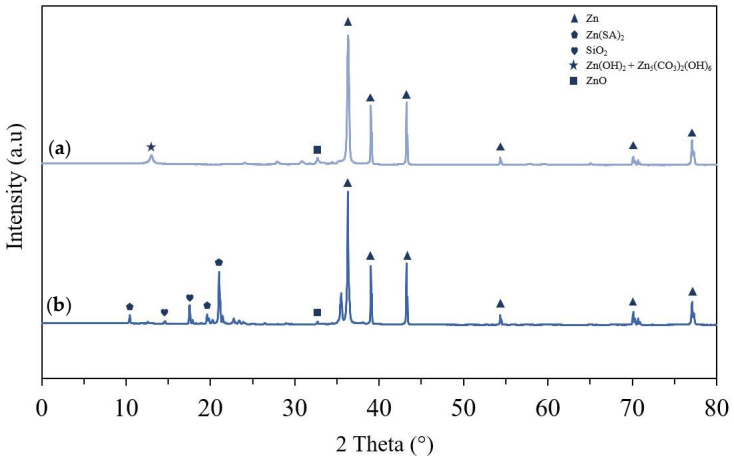

Figure 14. XRD patterns of humidity samples after 1000 h (**a**) uncoated sample and (**b**) hydrophobic sample.

FTIR analysis was completed alongside XRD to corroborate the observation of carbonate ($(CO_3)^{2-}$) bonds within the uncoated sample, this data is presented in Figure 15. This is highlighted by the peaks observed at 1500 and 1390 cm^{-1} relating to the antisymmetric stretching modes of $(CO_3)^{2-}$ [42]. This data provides validation that the white precipitate observed in Figure 11 can be mainly accounted to zinc carbonate hydroxide and zinc hydroxide formation on the surface. The mass change of both the uncoated and coated samples after humidity testing is assumed to be attributed to this and thus reinforces the theory that the coated sample has a higher resistance to corrosion due to a smaller change in mass.

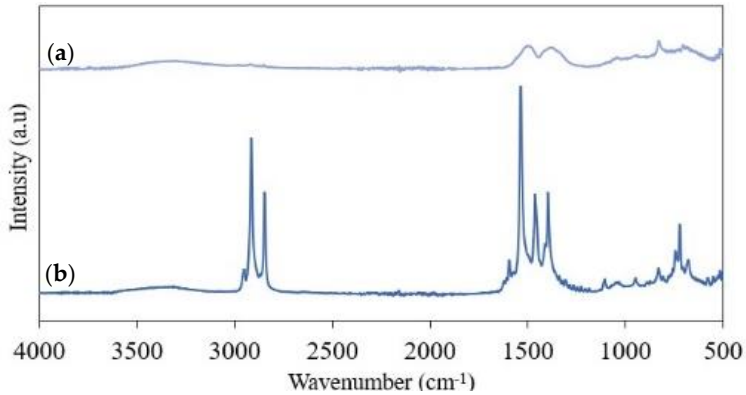

Figure 15. FTIR spectra of humidity samples after 1000 h: (**a**) uncoated surface and (**b**) hydrophobic surface.

4. Conclusions

A systematic study was employed to improve the processability of a one-step hydrophobic coating for HDG steel and to make it more industrially appropriate. The variables highlighted throughout the study included the immersion time, solvent used, addition of NaOH, molarity and SiO_2 particle size. The best-performing coating demonstrated a CA of 146° from an immersion time in formulation of 120 min. The formulation variables were IPA used as the solvent, 2% wt. 1 M NaOH (aq), 0.2 M stearic acid and micro-SiO_2 (0.2–0.3 µm).

Under standard accelerated exposure tests, the uncoated samples were seen to increase in mass by approximately three times the amount of the coated samples, thus, inferring that considerable corrosion resistance was gained from the coating. When comparing this methodology to other one-step processes by Li et al., we observed that, despite a longer processing time, the use of more commercially available, economically viable and safer constituents within the formulation justifies its development. The methodology displays significantly reduced health and safety risks and avoids the use of toxic chemical nitrates [6,26]. In comparison to Laing et al., the processing times were reduced by 67%, and the use of chemical additions, such as fumed silica, provided a vastly cheaper and safer alternative to nano-silica [13].

While the processing times were reduced by 67%, the process of creating hydrophobic coatings remains in hours not minutes. In practice, this means that it is suitable for batch processing only given that inline residence times require processing times in tens of seconds. The limiting factor is the kinetic rate of hydrothermal growth of the zinc stearate, and it has been demonstrated that this cannot be manipulated through changes in stearic acid solution concentration. Increases in temperature would be a natural step to increase the zinc stearate creation rate; however, this is limited by several factors.

The processing temperature is limited by the solvent boiling point, which, for ethanol and IPA, limits this to ~70 °C. Any further increase would risk boiling, altering the chemistry of the bath and producing a significant health and safety risk. Any change to a higher boiling point solvent would need to balance the solubility of the stearic acid and zinc stearate to ensure that the stearate can be added to the solution while retaining the insolubility (or sparing solubility) of the zinc stearate. L-butanol benefits from a higher boiling point (117 °C) and has stearic acid solubility similar to IPA [43]. Whether the potential increased operating temperature would be beneficial needs to be balanced with the safety and energy considerations.

Zinc is the dominant metal used in galvanising; however, it is also common that other alloying materials, such as magnesium and aluminium, are added to the metallic coating to further improve the corrosion resistance. The inclusion of these alloying compounds offers the possible formation of other metal-organic compounds as well as zinc stearate. The impact on hydrophobicity should also be investigated for these materials. This would help to identify the universality of the coating across the broad range of zinc-coated steel substrates. The coating demonstrated a significant improvement in corrosion resistance during industry standard humidity testing; however, the physical robustness also needs to be considered in any lifetime prediction. Further evaluation of the relative abrasion resistance and friction would be beneficial in estimating the real-world product lifetime extension provided by the zinc stearate coating.

Author Contributions: Conceptualization, J.W. and E.J.; methodology, J.W., C.G. and E.J.; validation, J.W., C.G., T.D. and E.J.; formal analysis, J.W., C.G., T.D. and E.J.; investigation, J.W. and C.G.; resources, E.J.; data curation, J.W. and E.J.; writing—original draft preparation, J.W., C.G. and E.J.; writing—review and editing, J.W., C.G. and E.J.; visualization, J.W.; supervision, C.G. and E.J.; project administration, E.J.; funding acquisition, E.J. All authors have read and agreed to the published version of the manuscript.

Funding: The authors would like to acknowledge the COATED M2A funding from the European Social Fund via the Welsh Government (WEFO), the EPSRC (through UKRI) (EP/S515218/1) and Tata Steel Europe that has made this research possible.

Institutional Review Board Statement: Not applicable.

Informed Consent Statement: Not applicable.

Data Availability Statement: The data used to support the findings of this study are included within the article and are available from the corresponding author upon request.

Acknowledgments: The authors would also like to thank Swansea University College of Engineering AIM facility, which was funded in part by the EPSRC (EP/M028267/1) and the European Regional Development Fund through the Welsh Government (80708) for the use of their Bruker D8 Discover.

Conflicts of Interest: The authors declare no conflict of interest.

References

1. Forget, L.; Delhalle, J.; Mekhalif, Z. Application of scanning Kelvin probe to study the corrosion protection of chromated hot-dip galvanized steel. *Mater. Corros.* **2001**, *52*, 181–184. [CrossRef]
2. Klimow, G.; Fink, N.; Grundmeier, G. Electrochemical studies of the inhibition of the cathodic delamination of organically coated galvanised steel by thin conversion films. *Electrochim. Acta* **2007**, *53*, 1290–1299. [CrossRef]
3. Long, Y.; Liu, C.; Peng, S. Enhanced performance of a green inorganic-based passive film on the batch hot-dip galvanized steel by organic additives. *Int. J. Electrochem. Sci.* **2020**, *15*, 2568–2580. [CrossRef]
4. Barati Darband, G.; Aliofkhazraei, M.; Khorsand, S.; Sokhanvar, S.; Kaboli, A. Science and Engineering of Superhydrophobic Surfaces: Review of Corrosion Resistance, Chemical and Mechanical Stability. *Arab. J. Chem.* **2020**, *13*, 1763–1802. [CrossRef]
5. Montemor, M.F. Functional and smart coatings for corrosion protection: A review of recent advances. *Surf Coat. Technol.* **2014**, *258*, 17–37. [CrossRef]
6. Li, C.; Ma, R.; Du, A.; Fan, Y.; Zhao, X.; Cao, X. Superhydrophobic Film on Hot-Dip Galvanized Steel with Corrosion Resistance and Self-Cleaning Properties. *Metals* **2018**, *8*, 687. [CrossRef]
7. Zhang, X.-F.; Chen, R.-J.; Hu, J.-M. Superhydrophobic surface constructed on electrodeposited silica films by two-step method for corrosion protection of mild steel. *Corros. Sci.* **2016**, *104*, 336–343. [CrossRef]
8. Vazirinasab, E.; Jafari, R.; Momen, G. Application of superhydrophobic coatings as a corrosion barrier: A review. *Surf. Coat. Technol.* **2018**, *341*, 40–56. [CrossRef]
9. Naing, T.H.; Rachpech, V.; Janudom, S.; Mahathaninwong, N. Characterization of water-repellent and corrosion-resistant superhydrophobic surfaces on galvanized steel. *J. Coat. Technol. Res.* **2020**, *17*, 1537–1548. [CrossRef]
10. Barthlott, W.; Neinhuis, C. Purity of the sacred lotus, or escape from contamination in biological surfaces. *Planta* **1997**, *202*, 1–8. [CrossRef]
11. Bahgat Radwan, A.; Abdullah, A.M.; Alnuaimi, N.A. Recent advances in corrosion resistant superhydrophobic coatings. *Corros. Rev.* **2018**, *36*, 127–153. [CrossRef]
12. Zhang, F.; Ju, P.; Pan, M.; Zhang, D.; Huang, Y.; Li, G.; Li, X. Self-healing mechanisms in smart protective coatings: A review. *Corros. Sci.* **2018**, *144*, 74–88. [CrossRef]
13. Liang, T.; Yuan, H.; Li, C.; Dong, S.; Zhang, C.; Cao, G.; Fan, Y.; Zhao, X.; Cao, X. Corrosion inhibition effect of nano–SiO_2 for galvanized steel superhydrophobic surface. *Surf. Coat. Technol.* **2021**, *406*, 126673. [CrossRef]
14. Latthe, S.S.; Sudhagar, P.; Devadoss, A.; Kumar, A.M.; Liu, S.; Terashima, C.; Nakata, K.; Fujishima, A. A mechanically bendable superhydrophobic steel surface with self-cleaning and corrosion-resistant properties. *J. Mater. Chem. A* **2015**, *3*, 14263–14271. [CrossRef]
15. Boinovich, L.; Gnedenkov, S.; Alpysbaeva, D.; Egorkin, V.; Emelyanenko, A.; Sinebryukhov, S.; Zaretskaya, A. Corrosion resistance of composite coatings on low-carbon steel containing hydrophobic and superhydrophobic layers in combination with oxide sublayers. *Corros. Sci.* **2012**, *55*, 238–245. [CrossRef]
16. Liu, Y.; Li, S.; Zhang, J.; Liu, J.; Han, Z.; Ren, L. Corrosion inhibition of biomimetic super-hydrophobic electrodeposition coatings on copper substrate. *Corros. Sci.* **2015**, *94*, 190–196. [CrossRef]
17. Yin, B.; Fang, L.; Hu, J.; Tang, A.-Q.; Wei, W.-H.; He, J. Preparation and properties of super-hydrophobic coating on magnesium alloy. *Appl. Surf. Sci.* **2010**, *257*, 1666–1671. [CrossRef]
18. Brassard, J.; Sarkar, D.; Perron, J.; Audibert-Hayet, A.; Melot, D. Nano-micro structured superhydrophobic zinc coating on steel for prevention of corrosion and ice adhesion. *J. Colloid Interface Sci.* **2015**, *447*, 240–247. [CrossRef]
19. Qian, B.; Shen, Z. Fabrication of Superhydrophobic Surfaces by Dislocation-Selective Chemical Etching on Aluminum, Copper, and Zinc Substrates. *Langmuir* **2005**, *21*, 9007–9009. [CrossRef]
20. Zhang, X.; Liang, J.; Liu, B.; Peng, Z. Preparation of superhydrophobic zinc coating for corrosion protection. *Colloids Surf. A Physicochem. Eng. Asp.* **2014**, *454*, 113–118. [CrossRef]

21. Xu, W.; Ning, T.; Yang, X.; Lu, S. Fabrication of superhydrophobic surfaces on zinc substrates. *Appl. Surf. Sci.* **2011**, *257*, 4801–4806. [CrossRef]
22. Hao, Y.; Soolaman, D.M.; Yu, H.-Z. Controlled Wetting on Electrodeposited Oxide Thin Films: From Hydrophilic to Superhydrophobic. *J. Phys. Chem. C* **2013**, *117*, 7736–7743. [CrossRef]
23. Liu, Q.; Chen, D.; Kang, Z. One-Step Electrodeposition Process to Fabricate Corrosion-Resistant Superhydrophobic Surface on Magnesium Alloy. *ACS Appl. Mater. Interfaces* **2015**, *7*, 1859–1867. [CrossRef] [PubMed]
24. Varshney, P.; Mohapatra, S.S.; Kumar, A. Superhydrophobic coatings for aluminium surfaces synthesized by chemical etching process. *Int. J. Smart Nano Mater.* **2016**, *7*, 248–264. [CrossRef]
25. Jurak, S.F.; Jurak, E.F.; Uddin, N.; Asmatulu, R. Functional Superhydrophobic Coating Systems for Possible Corrosion Mitigation. *Int. J. Autom. Technol.* **2020**, *14*, 148–158. [CrossRef]
26. Li, C.; Ma, R.; Du, A.; Fan, Y.; Zhao, X.; Cao, X. One-step fabrication of bionic superhydrophobic coating on galvanised steel with excellent corrosion resistance. *J. Alloys Compd.* **2019**, *786*, 272–283. [CrossRef]
27. Chen, Z.; Hao, L.; Chen, A.; Song, Q.; Chen, C. A rapid one-step process for fabrication of superhydrophobic surface by electrodeposition method. *Electrochim. Acta* **2012**, *59*, 168–171. [CrossRef]
28. Knudsen, O.Ø.; Forsgren, A. *Corrosion Control Through Organic Coatings*; CRC Press: Boca Raton, FL, USA, 2017.
29. Peißker, P. Surface-preparation technology. In *Handbook of Hot-Dip Galvanization*; John Wiley & Sons, Ltd.: Hoboken, NJ, USA, 2011; pp. 29–90.
30. Calvo, M.B.; Cepeda, E.A. Solubilities of Stearic Acid in Organic Solvents and in Azeotropic Solvent Mixtures. Available online: https://pubs.acs.org/sharingguidelines (accessed on 25 January 2022).
31. Heryanto, R.; Hasan, M.; Abdullah, E.C.; Kumoro, A.C. Solubility of stearic acid in various organic solvents and its prediction using non-ideal solution models. *ScienceAsia* **2007**, *33*, 469–472. [CrossRef]
32. Cassie, A.B.D.; Baxter, S. Wettability of porous surfaces. *Trans. Faraday Soc.* **1944**, *40*, 546–551. [CrossRef]
33. De Leon, A.; Advincula, R.C. Conducting polymers with superhydrophobic effects as anticorrosion coating. In *Intelligent Coatings for Corrosion Control*; Elsevier Inc.: Amsterdam, The Netherlands, 2015; pp. 409–430. Available online: https://app.knovel.com/web/view/khtml/show.v/rcid:kpICCC0001/cid:kt00U8P2E2/viewerType:khtml/root_slug:intelligent-coatings/url_slug:conducting-polymers-with?&b-toc-cid=kpICCC0001&b-toc-root-slug=intelligent-coatings&b-toc-title=IntelligentCoatingsforC (accessed on 11 May 2022).
34. Zouboy, N.D.E.; Pourbaix, M. *Atlas of Electrochemical Equilibria in Aqueous Solutions*; Pourbaix, M., Ed.; Pergamon Press: Oxford, UK, 1966; 406p.
35. Zhao, W.; Zhu, R.; Jiang, J.; Wang, Z. Environmentally-friendly superhydrophobic surface based on Al_2O_3@KH560@SiO_2 electrokinetic nanoparticle for long-term anti-corrosion in sea water. *Appl. Surf. Sci.* **2019**, *484*, 307–316. [CrossRef]
36. Mahadik, S.A.; Pedraza, F.; Vhatkar, R.S. Silica based superhydrophobic coating for long-term industrial and domestic applications. *J. Alloys Compd.* **2016**, *663*, 487–493. [CrossRef]
37. Yu, F.; Gao, J.; Liu, C.; Chen, Y.; Zhong, G.; Hodges, C.; Chen, M.; Zhang, H. Preparation and UV aging of nano-SiO_2/fluorinated polyacrylate polyurethane hydrophobic composite coating. *Prog. Org. Coat.* **2020**, *141*, 105556. [CrossRef]
38. Zeng, Y.; Qin, Z.; Hua, Q.; Min, Y.; Xu, Q. Sheet-like superhydrophobic surfaces fabricated on copper as a barrier to corrosion in a simulated marine system. *Surf. Coat. Technol.* **2019**, *362*, 62–71. [CrossRef]
39. Cao, L.; Wan, Y.; Li, Y.; Yang, S. Corrosion-resistant and friction-reducing performance of super-hydrophobic coating on hot-dip galvanised steel in a 3.5% NaCl solution. *Lubr. Sci.* **2021**, *33*, 325–334. [CrossRef]
40. Wahab, R.; Ansari, S.G.; Kim, Y.S.; Dar, M.A.; Shin, H.S. Synthesis and characterization of hydrozincite and its conversion into zinc oxide nanoparticles. *J. Alloys Compd.* **2008**, *461*, 66–71. [CrossRef]
41. Sun, H.; Liu, S.; Sun, L. A comparative study on the corrosion of galvanized steel under simulated rust layer solution with and without 3.5wt% NaCl. *Int. J. Electrochem. Sci.* **2013**, *8*, 3494–3509.
42. Winiarski, J.; Tylus, W.; Winiarska, K.; Szczygieł, I.; Szczygiel, B. XPS and FT-IR Characterization of Selected Synthetic Corrosion Products of Zinc Expected in Neutral Environment Containing Chloride Ions. *J. Spectrosc.* **2018**, *2018*, 2079278. [CrossRef]
43. Liu, W.J.; Sun, C.; Zhao, P.X.; Wang, S.F. Solubility of Stearic Acid in Ethanol, 1-Propanol, 2-Propanol, L-Butanol, Acetone, Methylene Chloride, Ethyl Acetate and 95% Ethanol from (293 to 315) K. *Adv. Mater. Res.* **2012**, *550–553*, 71–74. [CrossRef]